NANO EXPRESS   **Open Access**

Synthesis, characterization, and magnetic properties of monodisperse CeO$_2$ nanospheres prepared by PVP-assisted hydrothermal method

Sumalin Phokha[1], Supree Pinitsoontorn[1], Prae Chirawatkul[2], Yingyot Poo-arporn[2] and Santi Maensiri[3*]

Abstract

Ferromagnetism was observed at room temperature in monodisperse CeO$_2$ nanospheres synthesized by hydrothermal treatment of Ce(NO$_3$)$_3$·6H$_2$O using polyvinylpyrrolidone as a surfactant. The structure and morphology of the products were characterized by X-ray diffraction (XRD), Raman spectroscopy, transmission electron microscopy, high-resolution transmission electron microscopy, and field-emission scanning electron microscopy (FE-SEM). The optical properties of the nanospheres were determined using UV and visible spectroscopy and photoluminescence (PL). The valence states of Ce ions were also determined using X-ray absorption near edge spectroscopy. The XRD results indicated that the synthesized samples had a cubic structure with a crystallite size in the range of approximately 9 to 19 nm. FE-SEM micrographs showed that the samples had a spherical morphology with a particle size in the range of approximately 100 to 250 nm. The samples also showed a strong UV absorption and room temperature PL. The emission might be due to charge transfer transitions from the 4*f* band to the valence band of the oxide. The magnetic properties of the samples were studied using a vibrating sample magnetometer. The samples exhibited room temperature ferromagnetism with a small magnetization of approximately 0.0026 to 0.016 emu/g at 10 kOe. Our results indicate that oxygen vacancies could be involved in the ferromagnetic exchange, and the possible mechanism of formation was discussed based on the experimental results.

Keywords: CeO$_2$, Nanospheres, Dilute magnetic oxide, Ferromagnetism, Oxygen vacancies, Valence states

Background

Oxide-dilute magnetic semiconductors (O-DMSs) such as ZnO, TiO$_2$, SnO$_2$, and In$_2$O$_3$ doped with transition metal (TM) ions have recently attracted much attention due to their potential use in magneto-optoelectronic applications [1-3]. These O-DMSs are optically transparent and exhibit ferromagnetism (FM) at room temperature (RT) and even well above RT. Recently, TM-doped CeO$_2$ have been also reported to exhibit ferromagnetism at and above room temperature [4-10]. Unlike other O-DMSs, CeO$_2$ has a cubic structure with a lattice parameter $a = 0.54113$ nm [11] that will facilitate the integration of spintronic devices with advanced silicon microelectronic devices.

Early work on CeO$_2$-based O-DMSs was focused on thin films [4-6] and only a few works have been carried out on powders, bulk, or nanocrystalline form [9-12]. Tiwari et al. [4] firstly discovered room temperature ferromagnetism (RT-FM) in Ce$_{1-x}$Co$_x$O$_{2-\delta}$ ($x \leq 0.05$) films deposited on a LaAlO$_3$ (001) substrate by pulsed laser deposition (PLD) technique. These films are transparent in a visible regime and exhibit a very high Curie temperature (T_C) at approximately 740 to 875 K with large magnetic moments of 6.1 ± 0.2 to 8.2 ± 0.2 μ_B/Co. Following the work by Tiwari et al., Song et al. [5] reported successful fabrication of Ce$_{1-x}$Co$_x$O$_{2-\delta}$ ($x = 0.03$) thin films with (111) preferential orientation deposited on a Si (111) substrate by a PLD technique. Their deposited films show RT-FM with large magnetic moment of 5.8 μ_B/Co and coercivity of 560 Oe. The authors also showed that the films could be deposited on glass but with smaller magnetic moment and coercivity. These

* Correspondence: santimaensiri@g.sut.ac.th
[3]School of Physics, Institute of Science, Suranaree University of Technology, Nakhon Ratchasima 30000, Thailand
Full list of author information is available at the end of the article

results suggested that the FM in Co-doped CeO_2 depend not only on the doping concentration of transition element, but also on the microstructure of film, including its crystallization, defects, vacancies, etc. Vodungbo et al. [6] also reported FM in Co-doped CeO_2 thin films grown by PLD on $SrTiO_3$ and Si substrate. The films were ferromagnetic with a T_C above 400 K. These authors found that the amount of structural defects had a little effect on FM, but the presence of oxygen during the growth or annealing reduced drastically the FM, suggesting that oxygen vacancies played an important role in the magnetic coupling between Co ions, while Wen et al. [9] reported the ferromagnetism observed in pure and Co-doped CeO_2 powders. The RT-FM in pure CeO_2 originated from oxygen vacancies while a slight Co doping in CeO_2 caused a nearly two-order enhancement of saturation magnetization (M_s) to 0.47 emu/g as compared with the pure sample. The authors suggested that the large RT-FM observed in Co-doped CeO_2 powder originated from a combination effect of oxygen vacancies and Co doping. Similarly, Ou et al. [10] reported RT-FM for $Ce_{1-x}Co_xO_2$ ($0 < x < 0.10$) nanorods prepared by electrodeposition route. The nanorods were ferromagnetic with a high T_C of about 870 K and the largest M_s of 0.015 emu/g. They suggested that the RT-FM observed in Co-doped CeO_2 nanorods was adjusted by the structural defects including oxygen vacancies. The same behavior was found in nanoparticles of Fe-doped CeO_2 [11] with an M_s value of 0.0062 emu/g in 3 at % Fe prepared by a sol–gel method and Fe-doped CeO_2 [12] with an M_s value of 0.10 emu/g in 1 at % Fe prepared by the proteic sol–gel process. The authors suggested that the RT-FM originated from an exchange of F-center, which involved a combination of oxygen vacancies and TM doping.

Surprisingly, the researchers report RT-FM of undoping in different oxides, such as thin films of HfO_2 [13], TiO_2 and In_2O_3 [14], and nanoparticles of CeO_2, Al_2O_3, ZnO, In_2O_3, and SnO_2 [15], while the corresponding bulk samples are diamagnetic. Most recently, there are some studies reporting ferromagnetism observed in pure CeO_2 on powders, nanocrystalline, or cubes [16-18]. Liu et al. [16] studied the size-dependent ferromagnetism in CeO_2 powders synthesized by precipitation route. They found that ferromagnetism was observed only in sub-20-nm powders with an M_s value of 0.08 emu/g. Similarly, Chen et al. [17] reported RT-FM in CeO_2 nanoparticles prepared by thermal decomposition method with an M_s value of 0.12 emu/g. The authors showed that its crystallite size in nanometers would be ferromagnetic because of the large value of the surface-to-volume ratio, leading to the exchange interactions between electron spin moments that resulted from oxygen vacancies at the surface [4]. Recently, Ge et al. [18] observed

ferromagnetism in CeO_2 nanocubes with an M_s value of 0.0057 emu/g (an average size of 5.3 nm) prepared by a chemical method. They suggest that oxygen vacancy is essential for the formation of FM in CeO_2 nanocubes.

However, magnetic properties of monodisperse nanospheres of pure CeO_2 have not yet been reported. In this work, we report the ferromagnetism observed in monodisperse CeO_2 nanospheres with a particle size of approximately 200 nm synthesized by hydrothermal treatment of $Ce(NO_3)_3 \cdot 6H_2O$ using polyvinylpyrrolidone (PVP) as a surfactant. The technique of preparation and the effect of the type of cerium source on the crystallinity and morphology were investigated. The prepared samples were characterized by X-ray diffraction (XRD), Raman spectroscopy, field-emission scanning electron microscopy (FE-SEM), transmission electron microscopy (TEM), high-resolution transmission electron microscopy (HRTEM), UV and visible spectroscopy (UV–vis), and photoluminescence (PL). The valence states of Ce ions were also investigated by using X-ray absorption near edge spectroscopy (XANES), and the magnetic properties of the samples were determined using a vibrating sample magnetometer (VSM). The origin of RT-FM in this pure CeO_2 is also discussed.

Methods

In this study, cerium (III) nitrate hexahydrate, $Ce(NO_3)_3 \cdot 6H_2O$ (99.99% purity; Kanto Corporation, Portland, OR, USA); cerium (III) acetate hydrate, $Ce(CH_3CO_2)_3 \cdot xH_2O$ (99.9% purity; Sigma-Aldrich Corporation, St. Louis, MO, USA); cerium (III) chloride heptahydrate, $CeCl_3 \cdot 7H_2O$ (99.9% purity; Sigma-Aldrich Corporation); cerium (III) sulfate octahydrate, $Ce_2(SO_4)_3 \cdot 8H_2O$ (99.999% purity; Sigma-Aldrich Corporation); and PVP (Sigma-Aldrich Corporation) were used as starting materials. In a typical procedure, one gram of PVP was mixed with 40 mL of deionized water under vigorous magnetic stirring at room temperature (27°C) until a homogeneous solution was obtained. Subsequently, 3 mmol of cerium source was slowly added to the PVP solution under vigorous stirring at room temperature for 2 h, in order to obtain a well-dissolved solution. Throughout the whole process described, no pH adjustment was made. The homogeneous solution was transferred into a Teflon-lined stainless steel autoclave of 50-mL capacity and prepared at 160°C and 200°C for 12 h and 160°C and 200°C for 24 h. After the autoclave was cooled naturally to room temperature, the precipitate was collected and washed several times with distilled water. The final product was then dried in a vacuum at 80°C overnight. In addition, the as-prepared samples were also annealed in argon atmosphere at 400°C for 2 h to study the effect of oxygen vacancies on magnetic properties of the annealed samples.

The prepared samples were characterized using XRD, Raman spectroscopy, FE-SEM, TEM, HRTEM, UV–vis, PL, XANES, and VSM. A Philips X-ray diffractometer (Philips Tecnai, Amsterdam, The Netherlands) with CuKα radiation ($\lambda = 0.15406$ nm) was used to study the phases of the pure CeO_2 samples. The Raman spectra were recorded at room temperature using a triple spectrometer (Jobin Yvon/ Atago-Bussan T-64000, HORIBA Jobin Yvon S.A.S., Chilly-Mazarin, France). The morphology of the sample was obtained from TEM (JEM 2010 200 kV, JEOL Ltd., Akishima, Tokyo, Japan). FE-SEM was performed using a JEOL JSM-6335 F (JEOL Ltd.). The optical absorption spectrum was measured in the range of 200 to 800 nm using a UV-3101PC UV–vis-NIR scanning spectrometer (Shimadzu Corporation, Nakagyo-ku, Kyoto, Japan). PL was carried out on a luminescence spectrometer (PerkinElmer LS-55B, PerkinElmer Instrument, Waltham, MA, USA), using a Xenon lamp as the excitation source at room temperature. The Ce L_3 XANES spectrum was studied using XANES in transmission mode at the BL4 Station at Siam Photon Laboratory (Synchrotron Light Research Institute (Public Organization), SLRI) in Nakhon Ratchasima, Thailand. The magnetic measurements were performed at room temperature using a vibrating sample magnetometer (VSM 7403, Lakeshore, Westerville, OH. USA).

Results and discussion

XRD analysis

The XRD patterns of the samples prepared by hydrothermal reaction at 160°C for 12 h are shown in Figure 1a. The sample obtained with $CeCl_3 \cdot 7H_2O$ as the starting agent shows no XRD peaks, indicating that it is amorphous, whereas the sample from $Ce(NO_3)_3 \cdot 6H_2O$ exhibits XRD peaks that correspond to the (111), (200), (220), (311), (222), and (400) planes, which are consistent with the face-centered cubic fluorite structure of CeO_2 in the standard data from the Joint Committee on Powder Diffraction Standards (JCPDS) 34–0394, indicating that pure CeO_2 was successfully synthesized via these procedures.

In this study, we found that the type of cerium source has a great effect on the morphology of the final product. The cerium source from $Ce(NO_3)_3 \cdot 6H_2O$ shows that the sample consisted of sphere-like particles with diameters of 100 to 250 nm (Figure 1b), whereas other cerium sources such as $CeCl_3 \cdot 7H_2O$, $Ce(CH_3CO_2)_3 \cdot xH_2O$, and $Ce_2(SO_4)_3 \cdot 8H_2O$ resulted in irregular shapes and agglomerated particles as shown in Figure 1c,d,e, respectively. Therefore, it is clearly seen that cerium source from nitrate is most favorable for the formation of uniformly sized CeO_2 nanospheres. It is possible that the absorption of PVP molecules on various crystallographic planes of cerium source played a major role in determining the product morphology, due
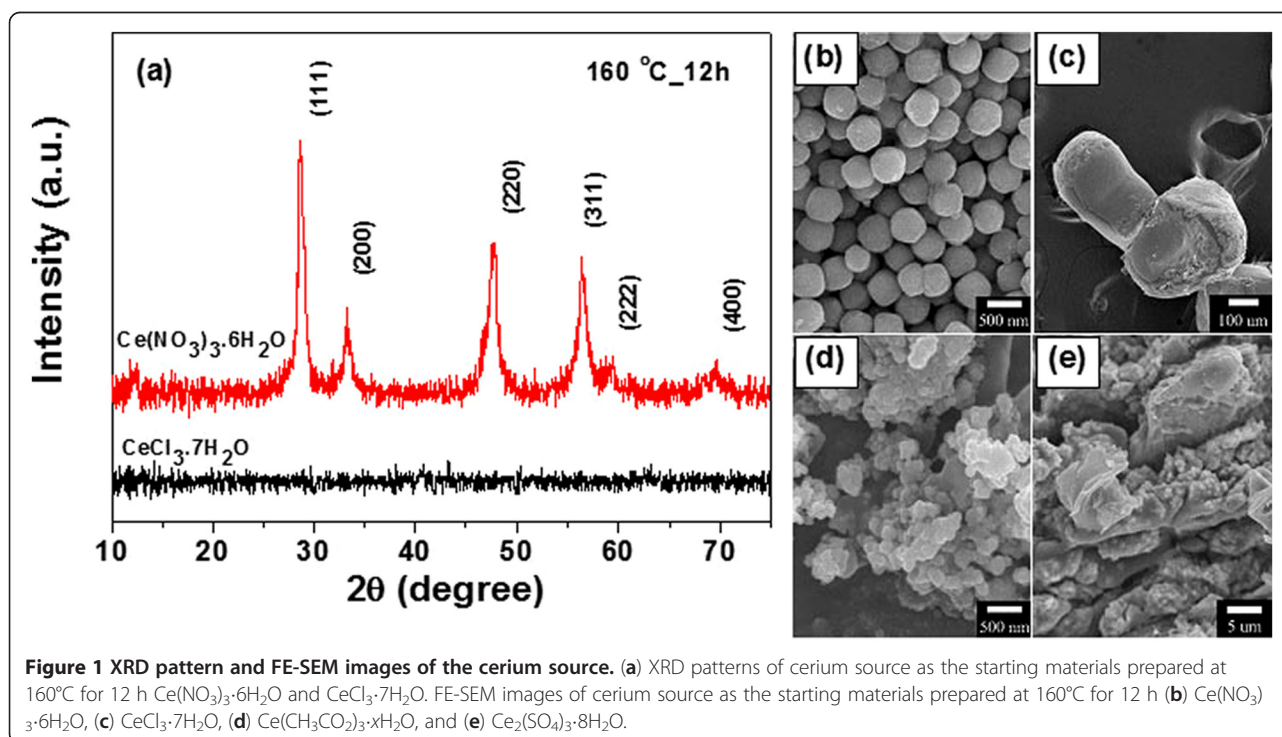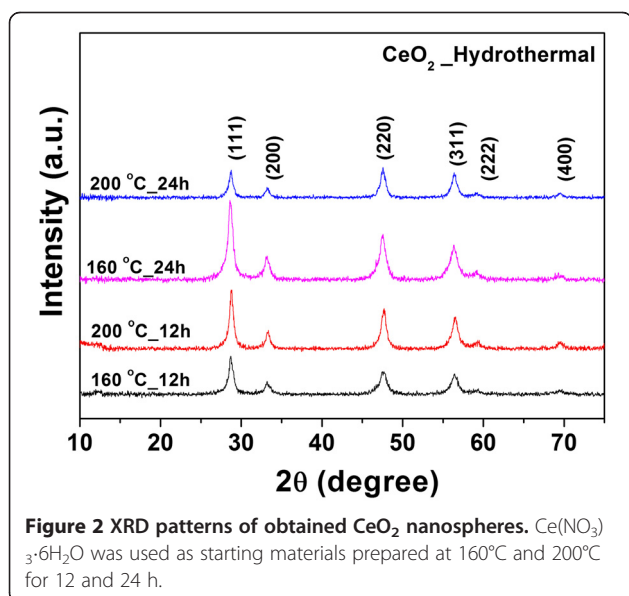

Figure 1 XRD pattern and FE-SEM images of the cerium source. (a) XRD patterns of cerium source as the starting materials prepared at 160°C for 12 h Ce(NO₃)₃·6H₂O and CeCl₃·7H₂O. FE-SEM images of cerium source as the starting materials prepared at 160°C for 12 h **(b)** Ce(NO₃)₃·6H₂O, **(c)** CeCl₃·7H₂O, **(d)** Ce(CH₃CO₂)₃·xH₂O, and **(e)** Ce₂(SO₄)₃·8H₂O.

to the fact that the supersaturation degree has a significant influence on the crystal nucleation rate and crystal growth rate [19]. However, the real reason for the morphology variation of the cerium source and surfactants has yet to be fully understood.

Figure 2 shows the XRD patterns of the pure CeO_2 from cerium nitrate at various hydrothermal treatment durations and temperatures. All the samples exhibited six typical peaks corresponding to the (111), (200), (220), (311), (222), and (400) planes, which are consistent with the face-centered cubic fluorite structure of CeO_2 in the standard data from JCPDS 34–0394, and this is in agreement with the selected area electron diffraction (SAED) patterns shown in Figure 3d. The values of the lattice constant calculated from the XRD spectra are shown in Table 1. The average crystallite size of all the samples was calculated from X-ray line broadening of the peaks at the (111), (200), (220), and (311) planes using Scherrer's equation, (as listed in Table 1). We observed that the lattice parameter decreases with increasing crystallite size. This decrease is possibly due to the introduction of Ce^{3+} ions into the crystal lattice. Ce^{3+} ions have a higher ionic radius (1.034 Å) compared with the Ce^{4+} ions (0.92 Å) and introduce oxygen vacancies. Therefore, the concentration of Ce^{3+} ions increases, and there is also an increase in the number of oxygen vacancies. It is observed that the pure CeO_2 nanoparticles experience considerable lattice distortion, which is in good agreement with earlier reports on CeO_2 nanoparticles [9,20], which indicated that this causes a change in the Ce-O bond length (lattice distortion) and the overall lattice parameter.

Figure 2 XRD patterns of obtained CeO₂ nanospheres. Ce(NO₃)₃·6H₂O was used as starting materials prepared at 160°C and 200°C for 12 and 24 h.

Raman analysis

The formation of a cubic structure in the CeO_2 nanospheres was further supported by the Raman spectra. Figure 4 shows typical spectra of CeO_2. The Raman active modes are shifted from 458 to 461 cm^{-1} for the CeO_2 samples heated at 160°C to 200°C. These Raman active modes are attributed to a symmetrical stretching mode of the Ce-80 vibrational unit, and therefore, they are very sensitive to any disorder in the oxygen sublattice that resulted from thermal, doping, or grain size [21-24]. The effect of the microstructure of CeO_2 on the shape of the Raman spectra was observed by the broadening of the line and by increases in its asymmetry, which are attributed to the reduction of the phonon lifetime in the nanocrystalline regime [25, 26]. The particle size of the CeO_2 sample can be also estimated from the Raman line broadening using the following Equation 1 [23, 24, 27]:

$$\Gamma(\text{cm}^{-1}) = 10 + \frac{124.7}{D_R}, \tag{1}$$

where $\Gamma(\text{cm}^{-1})$ is the full width at half maximum of the Raman active mode peak and D_R is the particle size of a CeO_2 sample. This relation can be used to determine the crystal size of the CeO_2 samples as shown in Table 1. This calculated crystal size is near that obtained from X-ray line broadening.

FE-SEM, TEM, and HRTEM analyses

The morphology and structure of CeO_2 nanospheres were investigated by FE-SEM and TEM as shown in Figure 3. TEM bright field images show that the samples contain monodisperse nanospheres with a narrow size distribution. The high-magnification TEM image of a single particle (Figure 3b) indicates that the sphere has a diameter of about 218 nm. This result is similar to the work reported by Zhou et al. [28], in which spherical CeO_2 crystallites assembled by nanoparticles were synthesized by hydrothermal treatment because small nanoparticles of CeO_2 aggregated and gradually evolved into a spherical assembly, achieving a low surface energy. The corresponding SAED patterns (inset in Figure 3d of the products show spotty ring patterns indicative of a face-centered cubic structure of CeO_2 (JCPDS 34–0394), which is in agreement with the XRD results. The HRTEM images of the CeO_2 sample prepared at 200°C for 12 h and the CeO_2 sample prepared at 200°C for 12 h followed by annealing in Ar at 400°C for 2 h, are shown in Figure 5a,b, respectively. The d spacings of the lattice fringes of approximately 0.30 and 0.31 nm for the CeO_2 sample prepared at 200°C for 12 h (Figure 5a) calculated from the HRTEM images correspond to
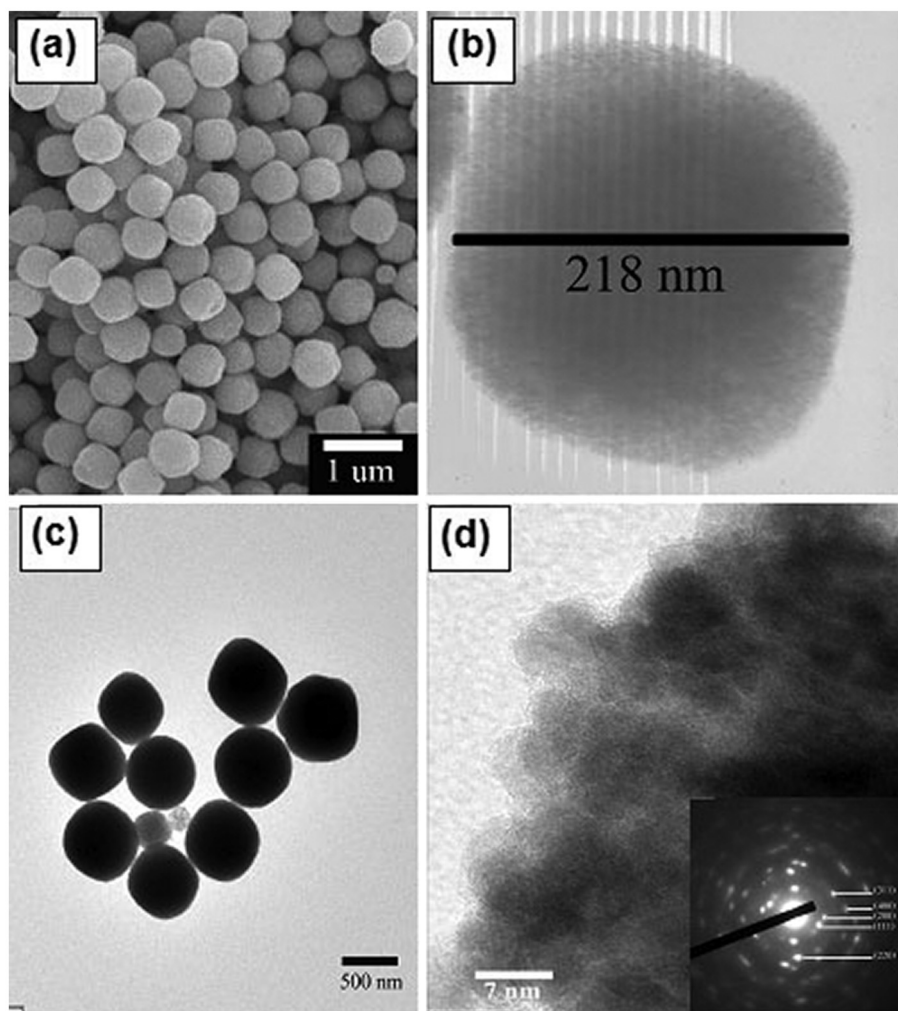
Figure 3 FE-SEM and TEM bright field images of CeO₂ nanospheres. (**a**) FE-SEM images of CeO₂ nanospheres prepared at 200°C for 24 h; (**b**) TEM bright field images of CeO₂ nanospheres prepared at 160°C for 12 h; (**c**) and (**d**) are TEM bright field images with corresponding SAED patterns (insets) of CeO₂ nanospheres prepared at 200X°C for 12 h.

the (111) plane of CeO_2, whereas the d spacings of approximately 0.31 and 0.32 nm (Figure 5b) for the CeO_2 sample prepared at 200°C for 12 h followed by annealing in Ar at 400°C for 2 h match with (111) plane of CeO_2. This is in good agreement with the standard data (JCPDS 34–0394).
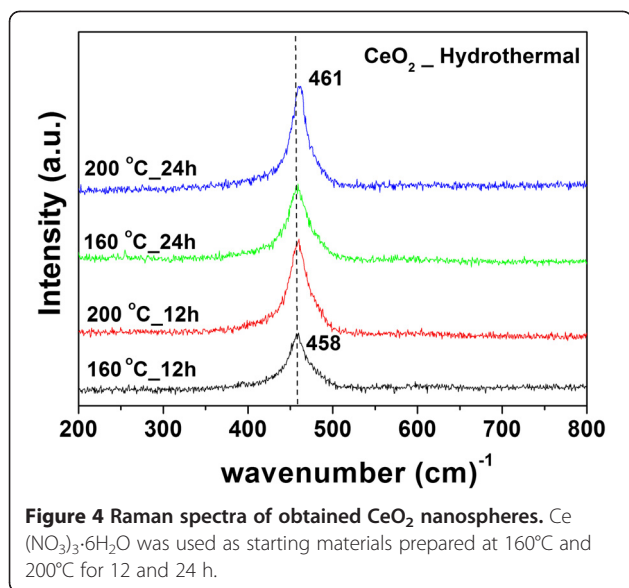
Optical properties

The UV–vis absorption spectra of the pure CeO_2 nanospheres are shown in Figure 6a. All the samples show a strong absorption below 400 nm (3.10 eV) with a well-defined absorbance peak at approximately 302 nm (4.10 eV). The direct bandgap energy (E_g) is determined

Table 1 Summary of crystallite sizes, lattice constant, bandgap, and magnetization of pure CeO₂ nanospheres

Sample	Crystallite size from XRD (nm)	Lattice constant a (nm)	E_g (eV)	Crystallite size from Raman spectroscopy (nm)	M_s at 10 kOe (emu/g)	
					Before Ar annealing	After Ar annealing
CeO₂ at 160 °C for 12 h	9.43 ± 0.41	0.5430 ± 0.0021	3.00	7.39	-	-
CeO₂ at 200 °C for 12 h	19.6 ± 0.53	0.5420 ± 0.0003	3.04	8.21	0.0026	0.011
CeO₂ at 160 °C for 24 h	12.2 ± 0.13	0.5430 ± 0.0003	3.06	9.23	0.0053	0.0026
CeO₂ at 200 °C for 24 h	15.6 ± 0.20	0.5428 ± 0.0006	3.10	12.28	0.016	0.015

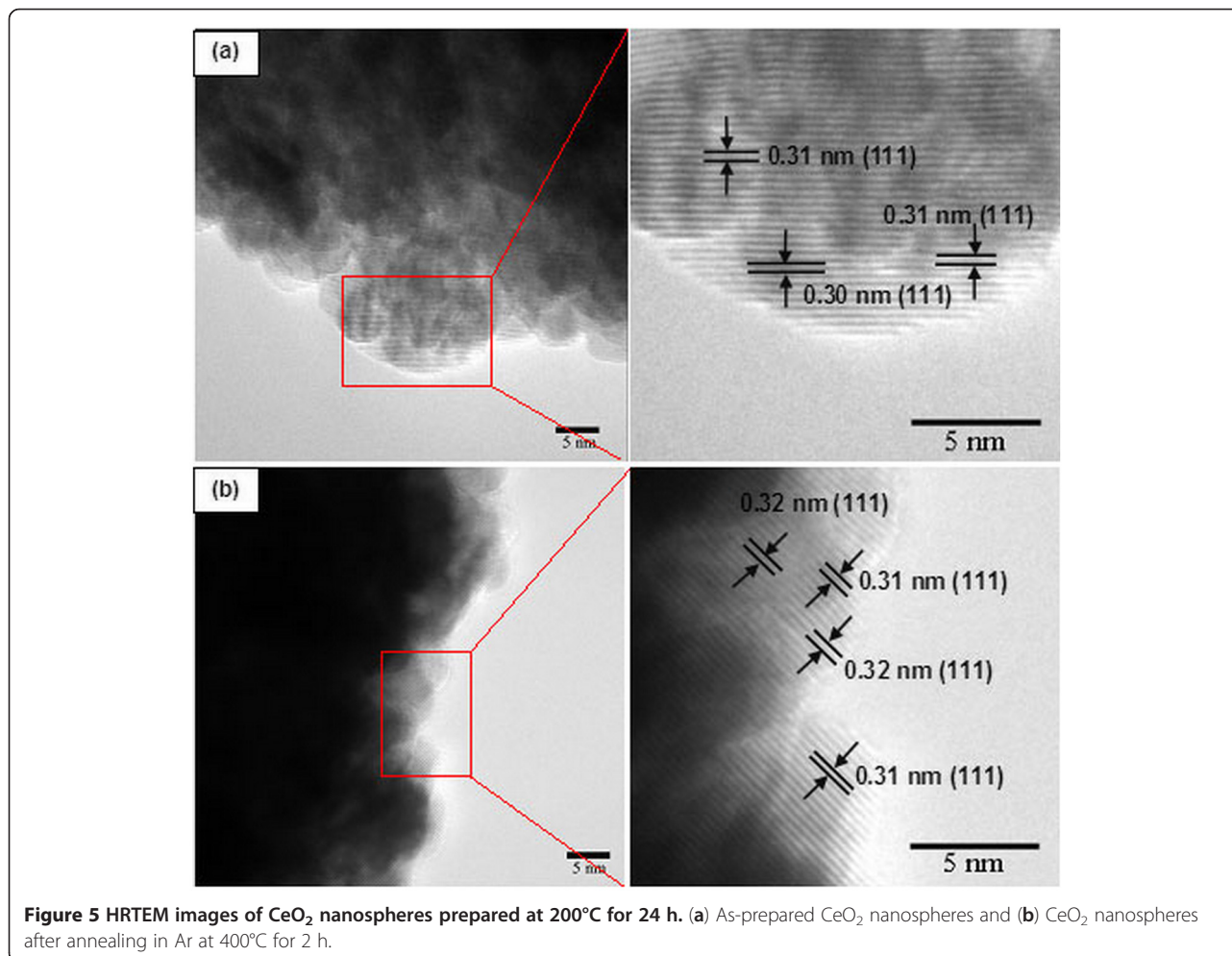E_g, bandgap energy; M_s, saturation magnetization. Data of magnetization of pure CeO₂ nanospheres is before and after Ar annealing.

Figure 4 Raman spectra of obtained CeO₂ nanospheres. Ce(NO₃)₃·6H₂O was used as starting materials prepared at 160°C and 200°C for 12 and 24 h.

by fitting the absorption data to the direct transition as shown in Equation 2:

$$\alpha h\nu = A\left(h\nu - E_{g}\right)^{1/2} \tag{2}$$

where α is the optical absorption coefficient, $h\nu$ is the photon energy, E_{g} is the direct bandgap, and A is a constant [29]. The extrapolation of the linear portions of the curves towards absorption equal to zero (y = 0) gives E_{g} for direct transitions (Figure 6b). The estimated direct bandgaps of all the samples are shown in Table 1. The bandgap of CeO₂ reported in this work is lower than that reported in the literature. Chen and Chang [30] reported direct bandgap values ranging from 3.56 to 3.71 eV for CeO₂ nanoparticles synthesized by precipitation method. Maensiri et al. [21] reported direct bandgap values ranging from 3.57 to 3.61 eV for CeO₂ nanoparticles synthesized by the sol–gel method using egg white. Similarly, Masui et al. reported direct bandgap values of 4.1 and 2.6 nm for CeO₂ nanoparticles prepared using reverse micelles to be 3.38 and 3.44 eV [31],
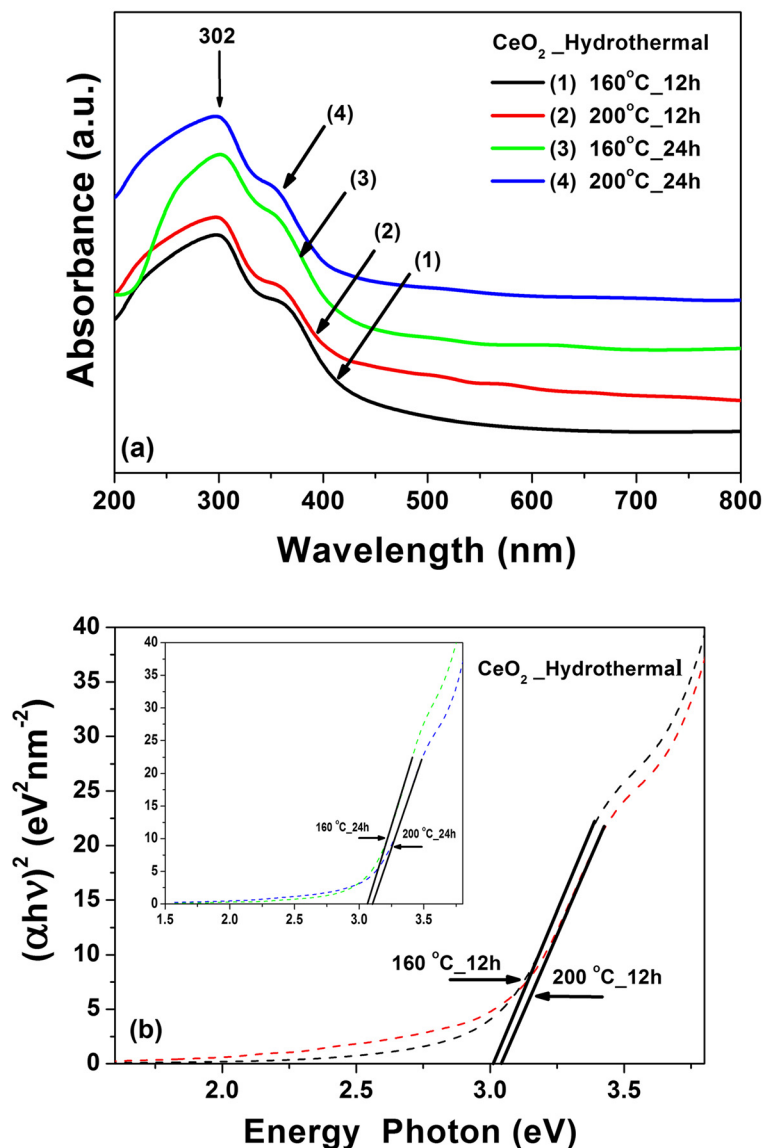

Figure 5 HRTEM images of CeO₂ nanospheres prepared at 200°C for 24 h. (**a**) As-prepared CeO₂ nanospheres and (**b**) CeO₂ nanospheres after annealing in Ar at 400°C for 2 h.

Figure 6 Room temperature optical absorbance spectra of CeO$_2$ nanospheres and plot of ($\alpha h\nu$)^2. (**a**) Room temperature optical absorbance spectra of CeO$_2$ nanospheres using Ce(NO$_3$)$_3$·6H$_2$O as starting materials. (**b**) Plot of ($\alpha h\nu$)^2 as a function of photon energy for the CeO$_2$ nanospheres.

respectively, due to quantum confinement effect [32]. This phenomenon has been well explained for particle sizes down to less than a few nanometers, but for our results, the bandgaps increased with increasing crystal size, which exhibit blueshifts in the UV absorption spectra inferred from the bandgap calculated for pure CeO$_2$ nanospheres. This blueshift has been reported to be an electrostatic potential effect due to a cerium valence change when the particle size is larger than a few nanometers (e.g., ≥8 nm). The Ce^{4+} ions coexist with Ce^{3+} ions, and these ions can be attributed to oxygen vacancies at the surface [33]. Therefore, in our work, the bandgaps increased with increasing crystal size. The crystallite size is in the range of 9 to 19 nm as indicated by the existence of the blueshift for our CeO$_2$ nanospheres.

PL analysis

Figure 7 shows the room temperature PL spectra obtained using a Xenon laser of 290 nm as the excitation source of the CeO$_2$ nanospheres. The spectra of all the samples are almost identical and mainly consist of five emission bands: a strong blue emission band at 422 nm (2.93 eV), a weak blue band at 446 nm (2.78 eV), a blue band at 460 nm (2.69 eV), a strong blue-green band at 485 nm (2.55 eV), and a green band at 529 nm
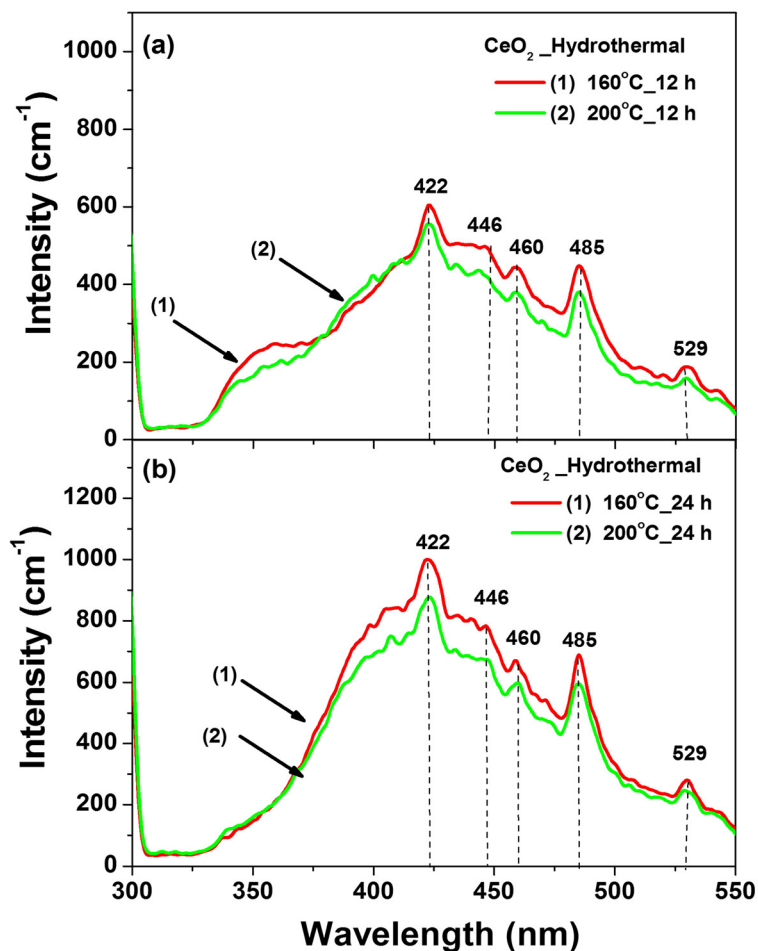
Figure 7 Room temperature photoluminescence spectrum of CeO$_2$ nanospheres using Ce(NO$_3$)$_3$·6H$_2$O as starting materials. The sample was dispersed in methanol and the excitation wavelength used in PL measurement was 290 nm.

(2.35 eV). Our results are consistent with that reported for CeO$_2$ in the literature. The strong emission peak at 410 nm [34] and 422 nm [35] observed for CeO$_2$ nanoparticles as-prepared at $\lambda_{ex} = 290$ nm. Maensiri et al. [21] reported a blue band at approximately 443 nm, along with a green band at 529 nm for 400°C to 500°C calcined sample, and a strong UV emission band at 392 nm for 600°C calcined sample. The dependence of the PL blue-shift peak on CeO$_2$ particle concentration has also been observed by Sathyamurthy et al. [34] for CeO$_2$ nanoparticles synthesized by a reverse micelle route. This phenomenon has been explained by charge transitions from the 4f band to the valence band of the CeO$_2$ in both nanoparticles and thin films [36]. In addition, it is well known that the emission energy from the 4f band to the valence band energy gap of CeO$_2$ is about 3.0 to 3.38 eV, as determined from the calculation of the electronic structure of CeO$_2$ [35,37]. Therefore, the emission in our CeO$_2$ samples could be assumed to be the transition from the Ce 4f band to the O 2p band (valence

band) in CeO$_2$. The broad PL band ranging from 300 to 550 nm of all the samples could be the result of defects, including oxygen vacancies in the crystal with electronic energy levels below the 4f band [38]. This is confirmed by the enhanced absorption tail below 3 eV in nonstoichiometric CeO$_2$ that was previously observed and attributed to the presence of oxygen vacancies [39].

XANES analysis

The valence state of Ce in pure CeO$_2$ nanospheres was determined by XANES spectra measured at Ce L$_3$ edge. Figure 8a shows the edge energies of the Ce (NO$_3$)$_3$·6H$_2$O standard and CeO$_2$ standard. The standard Ce(NO$_3$)$_3$·6H$_2$O has a single peak illustrated by one intense white line at approximately 5,726.8 eV, which can be associated with the final state of 2p4$f^1$5de$_g$L, where L denotes an oxygen ligand 2p hole, corresponding to the Ce^{3+} valence state [40]. In the standard CeO$_2$, there are four peaks comprising high energy peak A, main peak B, low energy peak C,
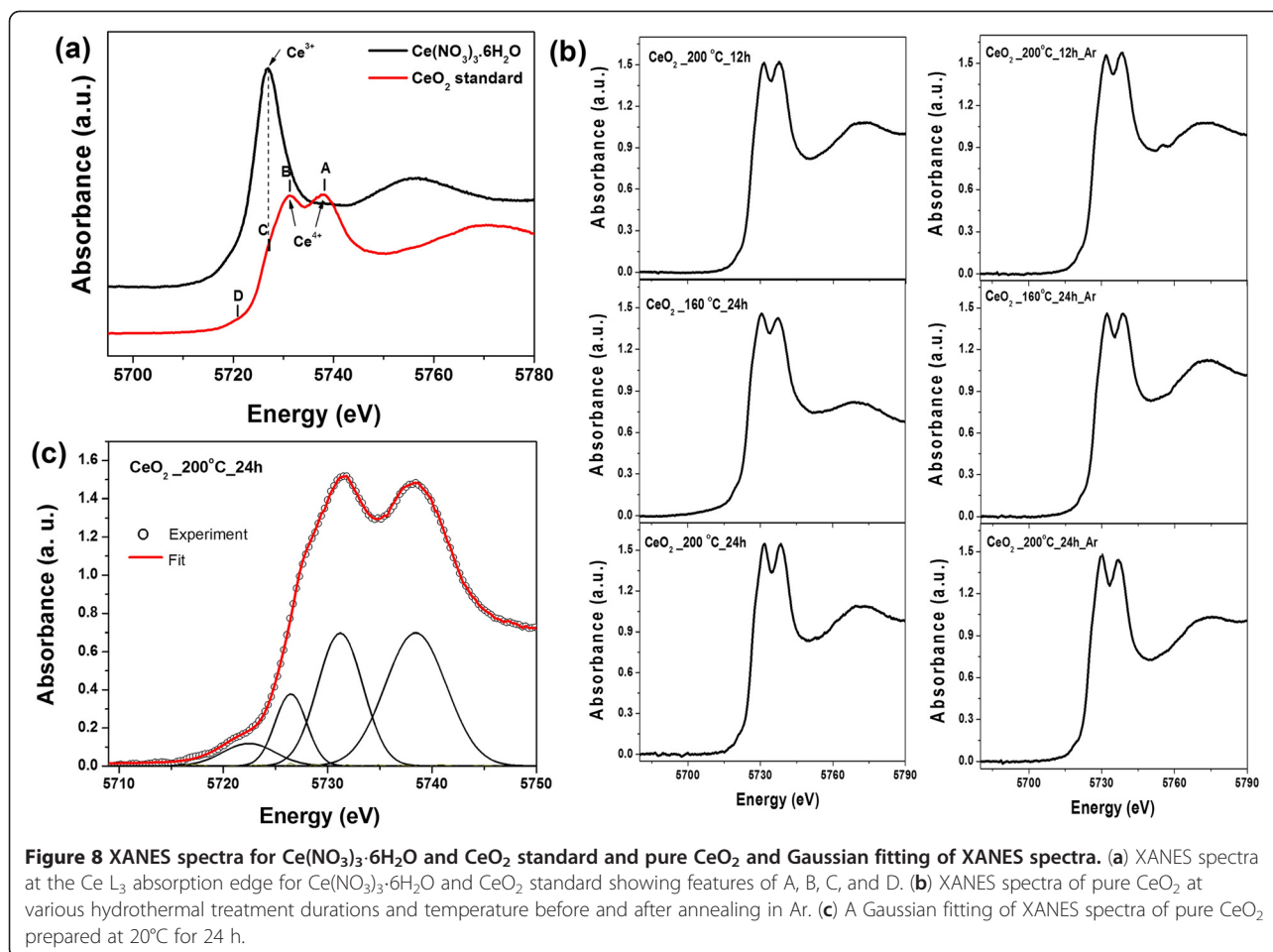
Figure 8 XANES spectra for Ce(NO₃)₃·6H₂O and CeO₂ standard and pure CeO₂ and Gaussian fitting of XANES spectra. (**a**) XANES spectra at the Ce L₃ absorption edge for Ce(NO₃)₃·6H₂O and CeO₂ standard showing features of A, B, C, and D. (**b**) XANES spectra of pure CeO₂ at various hydrothermal treatment durations and temperature before and after annealing in Ar. (**c**) A Gaussian fitting of XANES spectra of pure CeO₂ prepared at 20°C for 24 h.

and pre-edge peak D, which have been reported and assigned previously [41-43]. Peaks A and B are shifted to higher energies at approximately 5,737.9 and 5,731.3 eV, respectively, and were assigned as being due to a mixture of the multi-electron with the final state of $2\underline{p}4f^05d$ and $2\underline{p}4f^15dt_g\underline{L}$, respectively, which characterizes the Ce in the Ce^{4+} valence state [40]. Peak C, at approximately 5,726.8 eV, is observed at the same energy as the white line of a typical Ce (NO₃)₃·6H₂O standard, corresponding to the Ce^{3+} valence state. Peak D is assigned to the final states of $2\underline{p}5d$ with a delocalized d character at the bottom of the conduction band due to the cubic crystal-field splitting of Ce $5d$ states [44].

Figure 8b shows the XANES spectra of pure CeO₂ for various hydrothermal treatment durations and temperatures before and after annealing in Ar. The quantitative analysis of the valence state of Ce in each of the three states of the CeO₂ nanospheres was performed using multi-peak Gaussian fitting obtained from the XANES spectra, as shown in Figure 8c. The analysis shows that Ce in the samples is in a mixed

valence state of Ce^{3+} and Ce^{4+}. From these results, we can obtain the valence state of Ce according to the fitting parameters of the peak positions and areas listed in Table 2. It is observed that the percentage of Ce^{3+} ranges from 7% to 13.7% in the pure CeO₂ samples. These results provide confirmation of the formation of oxygen vacancies on the surface of the CeO₂ samples. It is possible that the concentration and distribution of oxygen vacancies play an important role in the magnetism of our CeO₂ nanospheres. The highest percentage of Ce^{3+} is 13.7% for CeO₂ prepared at 200°C for 24 h, with the increase in the number of oxygen vacancies, leading to the highest M_s values. The concentration of Ce^{3+} in our pure CeO₂ sample is higher than the values reported in the literature for CeO₂. Zhang et al. [41] reported the average Ce^{3+} concentration of 10- and 6-nm CeO₂ nanoparticles prepared by mixing cerium nitrate and hexamethylenetetramine in aqueous solution at room temperature to be 1% and 6.5%, respectively. Chen et al. [17] reported that the concentration of Ce^{3+} was higher than 21% for CeO₂ nanoparticles

Table 2 Gaussian fitting for percentage of Ce^{3+} of pure CeO_2 nanospheres before and after Ar annealing

Sample	Peak position (eV)		Peak area (eV)		Percentage of Ce^{3+} (%)	
	Before Ar annealing	After Ar annealing	Before Ar annealing	After Ar annealing	Before Ar annealing	After Ar annealing
CeO_2 at 200 °C for 12 h	5737.881	5738.471	5.128	5.672	7.8	12.4
	5730.733	5731.222	3.791	3.603		
	5724.617	5725.931	0.761	1.308		
CeO_2 at 160 °C for 24 h	5737.245	5738.888	6.734	4.703	9.8	10.4
	5729.911	5731.695	3.549	3.427		
	5726.128	5726.769	1.013	0.949		
CeO_2 at 200 °C for 24 h	5738.440	5736.924	5.154	5.713	13.7	13.3
	5731.205	5729.691	3.799	3.741		
	5726.465	5724.987	1.427	1.445		

synthesized by the thermal decomposition method, which is higher than the value for pure CeO_2 nanospheres reported in this study.

Magnetic properties

Figure 9a,b shows the field dependence of the specific magnetization (*M-H* curve) of pure CeO_2 samples prepared at 160°C and 200°C for 12 h and prepared at 160°C and 200°C for 24 h, respectively, obtained from room temperature VSM measurements. The sample of CeO_2 prepared at 160°C for 12 h exhibits mixed behaviors of ferromagnetism and diamagnetism having hysteresis loops at low field. The samples that were prepared at 200°C for 12 h showed weak RT-FM with magnetization (*M*) of approximately 0.0026 emu/g, and the samples that were prepared at 160°C and 200°C for 24 h showed weak RT-FM with saturation magnetization (M_s) of approximately 0.0053 and 0.016 emu/g, respectively (as listed in Table 1). These values are higher than the M_s values reported in the literature for pure CeO_2 nanospheres [15,17]. Sundaresan et al. [15] reported an RT-FM with an M_s value of approximately 0.0019 emu/g for CeO_2 nanoparticles with an average size of approximately 15 nm. Ge et al. [18] reported weak ferromagnetic behavior at an ambient temperature with an M_s value of approximately 0.0007 emu/g for pure CeO_2 nanoparticles with an average size of approximately 100 nm obtained commercially from Sigma-Aldrich Corporation (purity of 99.9%). However, magnetic behavior (M_s of approximately 0.0057 emu/g) was also observed in monodisperse CeO_2 nanocubes with an average size of approximately 5.3 nm prepared by a chemical method. The results obtained here (experimental and theoretical) provide evidence that pure CeO_2 samples can indeed have a magnetic moment due to oxygen vacancies. This direct ferromagnetic coupling is called *F*-center exchange (FCE) [45], as cerium can have both variable valence states (Ce^{4+}/Ce^{3+}) and oxygen vacancies on the surface of the CeO_2 nanoparticles. It is possible that oxygen vacancies can create magnetic moments on neighboring Ce ions [46]. In this work, the effect of Ar annealing at 400°C for 2 h on the magnetic properties was also performed to confirm the effect of oxygen vacancies on magnetic properties of the annealed samples. However, this effect was clearly observed only on the CeO_2 sample prepared at 200°C for 12 h and followed by annealing in argon atmosphere at 400°C for 2 h, as its magnetization increased from 0.0025 emu/g to 0.010 emu/g as (see inset of Figure 9b). It is noted that for the samples prepared at 160°C and 200°C for 24 h, annealing did not affect much their magnetic behavior due to the short time of annealing.

To explain the origin of the ferromagnetic contribution in the CeO_2 nanostructures, the following arguments are proposed. The annealing of samples in an Ar atmosphere at 400°C for 2 h could possibly increase the number of oxygen vacancies and Ce^{3+} ions in the samples. The high concentration of Ce^{3+} (approximately 13.3% Ce^{3+} for the sample prepared at 200 °C for 24 h) suggests that defects could be present in the majority of the samples, which activate more coupling between the Ce ions, leading to an increase in M_s. Wen et al. [9] reported the variation of RT-FM in oxygen and H_2 (10%)/Ar (90%) annealed samples of 1% Co-doped CeO_2 powder. They found that the sample showed little hysteresis loop after O_2 annealing and that the FM signal decreased significantly, while the H_2 (10%)/Ar (90%) annealed sample showed an enhanced FM with M_s of about 0.4 emu/g. However, further work is needed to achieve a thorough understanding, and this will be of
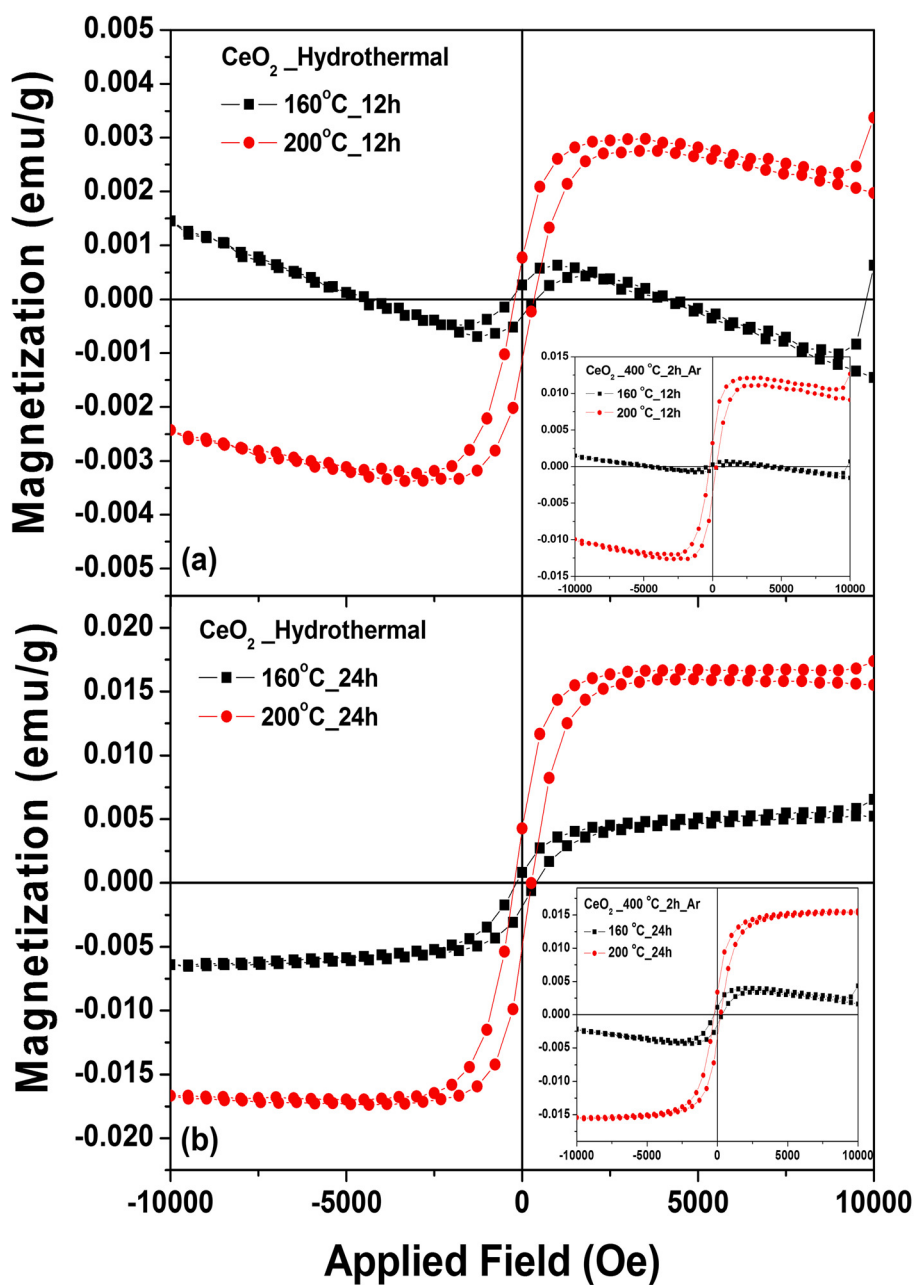
Figure 9 Magnetic properties of monodisperse CeO$_2$ nanospheres. Prepared at (**a**) 160℃ and 200℃ for 12 h and (**b**) 160℃ and 200℃ for 24 h. Inset shows CeO$_2$ samples after annealing in argon atmosphere at 400℃ for 2 h.

great interest to researchers in the field of dilute magnetic oxides.

Conclusions

In summary, spheres of pure CeO$_2$ with Ce(NO$_3$)$_3$·6H$_2$O using PVP as a surfactant have been successfully synthesized by hydrothermal method, and their structures, valence state, and magnetic properties were investigated. The XRD and Raman spectroscopy results suggested the formation of CeO$_2$ cubic fluorite structures in the CeO$_2$ samples, which was in agreement with the SAED patterns. It is observed that there is a decrease in the lattice parameters with increasing crystallite size, possibly due to the formation of structure defects/oxygen vacancies in the CeO$_2$ lattice. The bandgaps of our CeO$_2$ nanospheres increased with increasing crystal size indicated by the existence of a blueshift due to a cerium valence change, and this can be attributed to oxygen vacancies at the surface. The surface defects in the CeO$_2$ nanospheres play an important role in the PL properties of

our sample. The XANES results reveal that a fraction of the Ce ions are in the 3+ state, and these cause the samples to show weak RT-FM with an M_s value of 0.0026 to 0.016 emu/g. A ferromagnetic exchange mechanism in the pure CeO_2 samples is discussed by FCE, and the M_s of samples was shown to change, as well as the proportion of oxygen vacancies.

Competing interests

The authors declare that they have no competing interests.

Authors' contributions

SP designed and carried out all the experiments and data analysis, and participated in preparing the draft of the manuscript. SP co-supervised the research and offered technical support for TEM. PC and YP offered technical support for XANES measurement and analysis. SM, the project coordinator, supervised the research, designed the experiments, participated in preparing the draft of the manuscript, and revised the manuscript. All authors read and approved the final manuscript.

Author details

[1]Department of Physics, Faculty of Science, Khon Kaen University, Khon Kaen 40002, Thailand. [2]Synchrotron Light Research Institute (Public Organization), Suranaree University of Technology, Nakhon Ratchasima 30000, Thailand. [3]School of Physics, Institute of Science, Suranaree University of Technology, Nakhon Ratchasima 30000, Thailand.

References

1. Prellier W, Fouchet A, Mercey B: **Oxide-diluted magnetic semiconductors: a review of the experimental status.** *J Phys Condens Matter* 2003, **15**:R1583.
2. Pearton SJ, Heo WH, Ivill M, Norton DP, Steiner T: **Dilute magnetic semiconducting oxides.** *Semicond Sci Technol* 2004, **19**:R59.
3. Coey JMD: **Dilute magnetic oxides.** *Curr Opin Solid State Mater Sci* 2006, **10**:83.
4. Tiwari A, Bhosle VM, Ramachandran S, Sudhakar N, Narayan J, Budak S, Gupta A: **Ferromagnetism in Co doped CeO_2: observation of a giant magnetic moment with a high Curie temperature.** *Appl Phys Lett* 2006, **88**:142511.
5. Song YQ, Zhang HW, Wen QY, Li YX, Xiao JQ: **Room-temperature ferromagnetism of Co-doped CeO_2 thin films on Si(111) substrates.** *Chin Phys Lett* 2007, **24**:218.
6. Vodungbo B, Zheng Y, Vidal F, Demaille D, Etgens VH, Mosca DH: **Room temperature ferromagnetism of Co doped $CeO_{2-\delta}$ diluted magnetic oxide: Effect of oxygen and anisotropy.** *Appl Phys Lett* 2007, **90**:062510.
7. Fernandes V, Klein JJ, Mattoso N, Mosca DH, Silveira E, Ribeiro E, Schreiner WH, Varalda J, de Oliveira AJA: **Room temperature ferromagnetism in Co-doped CeO_2 films on Si(001).** *Phys Rev B* 2007, **75**:121304R.
8. Thurber A, Reddy KM, Shutthanandan V, Engelhard MH, Wang C, Hays J, Punnoose A: **Ferromagnetism in chemically synthesized CeO_2 nanoparticles by Ni doping.** *Phys Rev B* 2007, **76**:165206.
9. Wen QY, Zhang HW, Song YQ, Yang QH, Zhu H, Xiao JQ: **Room-temperature ferromagnetism in pure and Co doped CeO_2 powders.** *J Phys Condens Matter* 2007, **19**:246205.
10. Ou YN, Li GR, Liang JH, Feng ZP, Tong YX: **$Ce_{1-x}Co_xO_{2-\delta}$ nanorods grown by electrochemical deposition and their magnetic properties.** *J Phys Chem C* 2010, **114**:13509–13514.
11. Paula CAB, Daniel AAS, Jose' GSD, Marcelo AM: **Structural and magnetic study of Fe-doped CeO_2.** *Physica B* 2010, **405**:1821–1825.
12. Maensiri S, Phokha S, Laokul P, Seraphin S: **Room temperature ferromagnetism in Fe-doped CeO_2 nanoparticles.** *J Nanosci Nanotechnol* 2009, **9**:6415–6420.
13. Venkatesan M, Fitzgerald CB, Coey JMD: **Thin films: unexpected magnetism in a dielectric oxide.** *Nature* 2004, **430**:630.
14. Coey JMD, Venkatesan M, Stamenov P, Fitzgerald CB, Dorneles LS: **Magnetism in hafnium dioxide.** *Phys Rev B* 2005, **72**:024450.
15. Sundaresan A, Bhargavi R, Rangarajan N, Siddesh U, Rao CNR: **Ferromagnetism as a universal feature of nanoparticles of the otherwise nonmagnetic oxides.** *Phys Rev B* 2006, **74**:161306R.
16. Liu Y, Lockman Z, Aziz A, Macmanus DJ: **Size dependent ferromagnetism in cerium oxide (CeO_2) nanostructures independent of oxygen vacancies.** *J Phys Condens Matter* 2008, **20**:165201.
17. Chen SY, Lu YH, Huang TW, Yan DC, Dong CL: **Oxygen vacancy dependent magnetism of CeO_2 nanoparticles prepared by thermal decomposition method.** *J Phys Chem C* 2010, **114**:19576–19581.
18. Ge MY, Wang H, Liu EZ, Liu JF, Jiang JZ, Li YK, Xu ZA, Li HY: **On the origin of ferromagnetism in CeO_2 nanocubes.** *Appl Phys Lett* 2008, **93**:062505.
19. Lu X, Li X, Chen F, Ni C, Chen Z: **Hydrothermal synthesis of prism-like mesocrystal CeO_2.** *J Alloys Comp* 2009, **476**:958–962.
20. Deshpande S, Patil S, Kuchibhatla SVNT, Seal S: **Size dependency variation in lattice parameter and valency states in nanocrystalline cerium oxide.** *Appl Phys Lett* 2005, **87**:133113.
21. Maensiri S, Marsingboon C, Loakul P, Jareonboon W, Promarak V, Anderson PL, Seraphin S: **Egg white synthesis and photoluminescence of platelike clusters of CeO_2 nanoparticles.** *Cryst Growth Des* 2007, **7**:950–955.
22. Phoka S, Laokul P, Swatsitang E, Promarak V, Seraphinc S, Maensiri S: **Synthesis, structural and optical properties of CeO_2 nanoparticles synthesized by a simple polyvinyl pyrrolidone (PVP) solution route.** *Mater Chem Phys* 2009, **115**:423–428.
23. Kosacki I, Suzuki T, Petrovsky V, Anderson HU, Colomban P: **Raman scattering and lattice defects in nanocrystalline CeO_2 thin films.** *Solid State Ionics* 2002, **149**:99–105.
24. Kosacki I, Petrovsky V, Anderson HU, Colomban P: **Raman spectroscopy of nanocrystalline ceria and zirconia thin films.** *J Am Ceram Soc* 2002, **85**:2646–2650.
25. Lee SH, Lu ZY, Babu SV, Matijevic E: **Chemical mechanical polishing of thermal oxide films using silica particles coated with ceria.** *J Materials Res* 2002, **7**:2744.
26. Laberty-Robert C, Long JW, Lucas EM, Pettigrew KA, Stroud RM, Doescher MS, Rolison DR: **Sol–gel derived ceria nanoarchitectures: synthesis, characterization and electrical.** *Chem Mater* 2006, **18**:50–58.
27. Weber WH, Hass KC, McBride JR: **Raman study of CeO_2: second-order scattering, lattice dynamics and particle-size effects.** *Phys Rev B* 1993, **48**:178–185.
28. Zhou F, Ni X, Zhang Y, Zheng H: **Size-controlled synthesis and electrochemical characterization of spherical CeO_2 crystallites.** *J Coll Interf Sci* 2007, **307**:135–138.
29. Ziegler E, Heinrich A, Oppermann H, Stover G: **Electrical properties and non-stoichiometry in ZnO single crystals.** *Phys Status Solidi A* 1981, **66**:635.
30. Chen HI, Chang HY: **Synthesis of nanocrystalline cerium oxide particles by the precipitation method.** *Ceram Int* 2005, **31**:795–802.
31. Masui T, Fujiwara K, Machida K, Adachi G, Sakata T, Mori H: **Characterization of cerium(IV) oxide ultrafine particles prepared using reversed micelles.** *Chem Mater* 1997, **9**:2197–2204.
32. Tsunekawa S, Wang JT, Kawazoe Y, Kasuya A: **Blueshifts in the ultraviolet absorption spectra of cerium oxide nanocrystallites.** *J Appl Phys* 2003, **94**:3654.
33. Barreca D, Bruno G, Gasparotto A, Losurdob M, Tondello E: **Nanostructure and optical properties of CeO2 thin films obtained by plasma-enhanced chemical vapor deposition.** *Mater Sci Eng C* 2003, **23**:1013–1016.
34. Sathyamurthy S, Leonard KJ, Dabestani RT, Paranthaman MP: **Reverse micellar synthesis of cerium oxide nanoparticles.** *Nanotechnology* 2005, **16**:1960–1964.

35. Yu SH, Colfen H, Fischer A: **High quality CeO₂ nanocrystals stabilized by a double hydrophilic block copolymer.** *Colloids Surfaces A Physicochem Eng Aspects* 2004, **243**:49–52.
36. Gao F, Li GH, Zhang JH, Qin FG, Yao ZY, Liu ZK, Wang ZG, Lin LY: **Growth and photoluminescence of epitaxial CeO₂ films on Si (111) substrate.** *Chin Phys Lett* 2001, **18**:443.
37. Morshed AH, Moussa ME, Bedair SM, Leonard R, Liu SX, Masry NE: **Violet/blue emission from epitaxial cerium oxide films on silicon substrates.** *Appl Phys Lett* 1997, **70**:1647.
38. Marabelli F, Wachter P: **Covalent insulator CeO₂: optical reflectivity measurements.** *Phys Rev B* 1987, **36**:1238–1243.
39. Koelling DD, Boring AM, Wood JH: **The electronic structure of CeO₂ and PrO₂.** *Solid State Commun* 1983, **47**:227–232.
40. Hormes J, Pantelouris M, Balazs GB, Rambaby B: **X-ray absorption near edge structure (XANES) measurements of ceria-based solid electrolytes.** *Solid State Ionics* 2000, **136–137**:945–954.
41. Zhang F, Wang P, Koberstein J, Khalid S, Chan SW: **Cerium oxidation state in ceria nanoparticles studied with X-ray photoelectron spectroscopy and absorption near edge spectroscopy.** *Surf Sci* 2004, **563**:74–82.
42. Beck DD, Capehart TW, Hoffman RW: **Determination of Ce valence in Rh-Ce/Al₂O₃ catalysts by X-ray absorption.** *Chem Phys Lett* 1989, **159**:205–213.
43. Shahin AM, Grandjean F, Long GJ, Schuman TP: **Cerium L3-edge XAS investigation of the structure of crystalline and amorphous cerium oxides.** *Chem Mater* 2005, **17**:315–321.
44. Zhang J, Wu Z, Liu T, Hu T, Wu Z, Ju X: **XANES study on the valence transitions in cerium oxide nanoparticles.** *J Synchrotron Rad* 2001, **8**:531–532.
45. Coey JMD, Douvalis AP, Fitzgerald CB, Venkatesan M: **Ferromagnetism in Fe-doped SnO₂ thin films.** *Appl Phys Lett* 2004, **84**:1332.
46. Esch F, Fabris S, Zhou L, Montini T, Africh C, Fornasiero P, Comelli G, Renzo R: **Electron localization determines defect formation on ceria substrates.** *Science* 2005, **309**:752–755.